Supplemental Material

Intrapericardial exosome therapy dampens cardiac injury via activating Foxo3

Running title: Intrapericardial exosomes repair heart via Foxo3

Dashuai Zhu[1,2,†], Shuo Liu[1,2,†], Ke Huang[1,2,†], Zhenzhen Wang[1,2], Shiqi Hu[1,2], Junlang Li[1,2], Zhenhua Li[1,2], Ke Cheng[1,2*]

[1]Department of Molecular Biomedical Sciences, North Carolina State University, Raleigh, NC 27606, USA

[2]Joint Department of Biomedical Engineering, University of North Carolina at Chapel Hill & North Carolina State University, Raleigh, NC 27606, USA

[*]Correspondence

[†]Contributed equally

Address for Correspondence:

Ke Cheng, PhD

Dept. of Molecular Biomedical Sciences, NC State University

Dept. of Biomedical Engineering, UNC-Chapel Hill & NC State University

Division of Molecular Pharmaceutics, UNC-Chapel Hill

1001 William Moore Drive, Raleigh, North Carolina 27607, United States

Tel: 919-513-6157

Fax: 919-513-7301

Email: ke_cheng@unc.edu

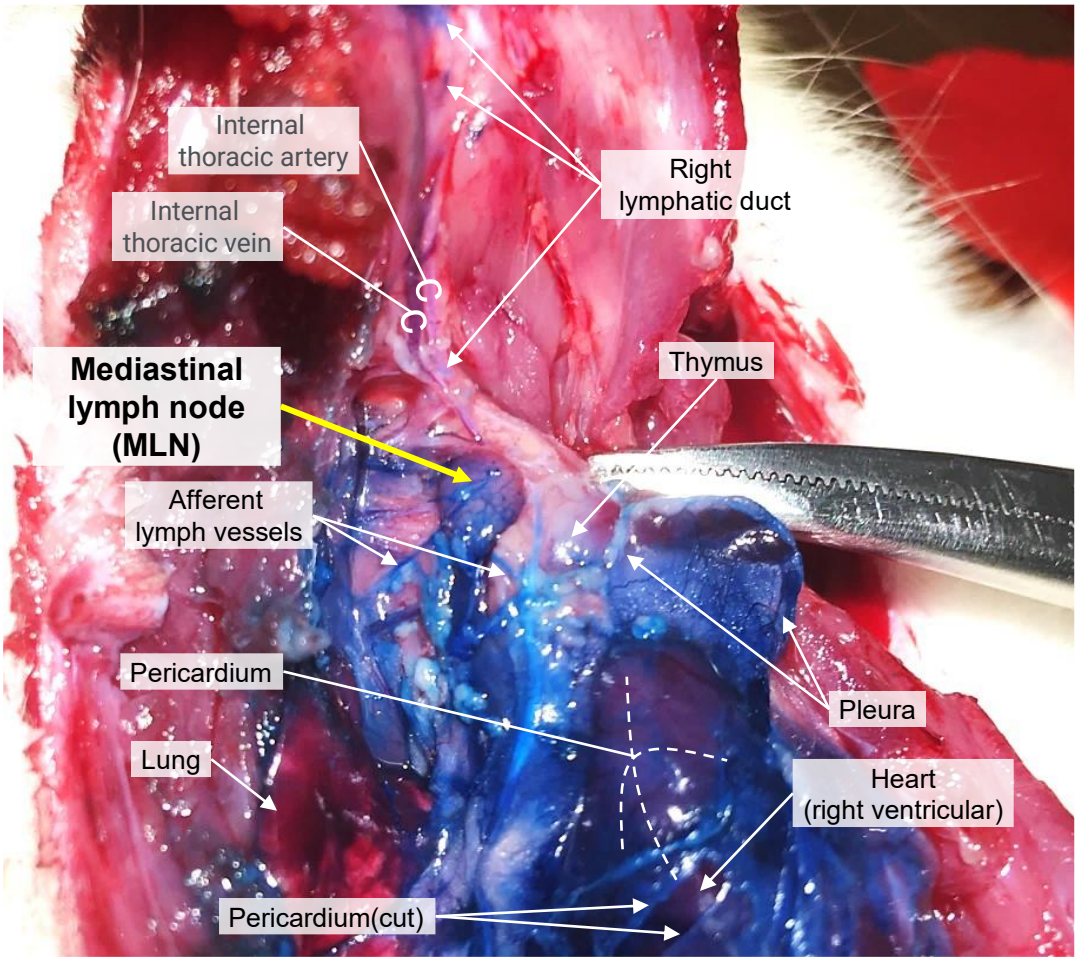

Fig. S1. Pericardial fluid drainage into mediastinal lymph node. 1% (w/v) Alician blue dye solution was injected into the pericardial cavity, after 1 hour drainage, the diffusion of the blue dye into the cardiac draining lymph node is observed (yellow arrow). The pericardium and the afferent lymph vessels aided in the dye transit.

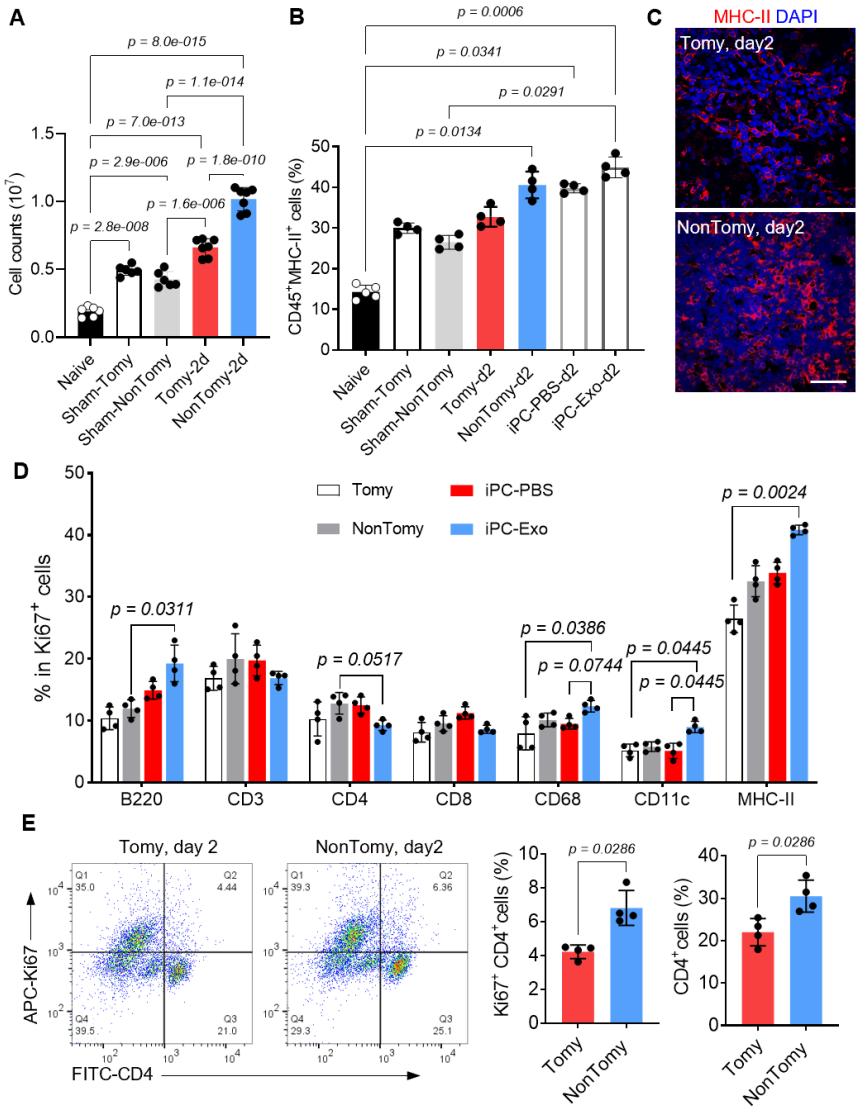

Fig. S2. Analysis of cell counts and cellular proliferation in the MLN. (**A**) Cell counts analysis in naïve, sham and MI rats. Each dot represents one lymph node. (**B**) Detection of antigen-presenting cells trafficking in rats of indicated groups. Each dot represents one animal. (**C**) Immunostaining detection of MHC-II$^+$ cells in the mediastinal lymph node. Scale bar, 60 μm. **(D)** Quantitative analysis of cellular proliferation in the mediastinal lymph node. n=4 animals for each group. **(E)** Detection of CD4$^+$ T cell proliferation in Tomy and NonTomy MI rats and the quantitative data. n=4 animals for each group. All the quantitative data was shown as mean ± SD. *p* value was determined by one-way ANOVA with Tukey's correction for A; Kruskal-Wallis's test with Dunn's correction for B, D; and by unpaired 2-tailed nonparametric Mann-Whitney test for E.

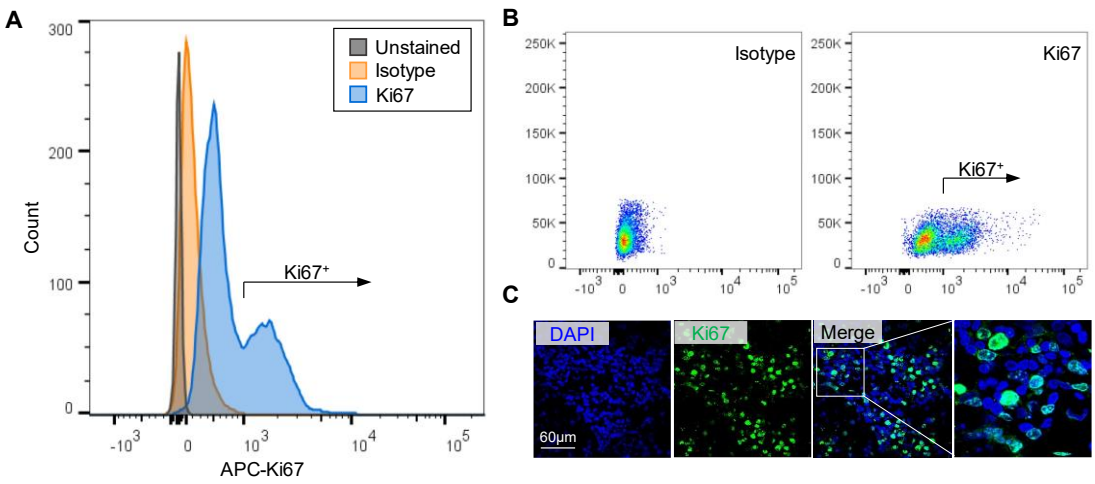

Fig. S3. Isotype staining for ki67 detection by flow cytometry. (A) Isotype staining was introduced by using rat IgG isotype control, and the histogram indicated the reliability of Ki67 antibody. (B) Pseudocolor images of the flow cytometry results. (C) Immunofluorescence staining of Ki67 in the lymph node. Scale bar, 60 μm.

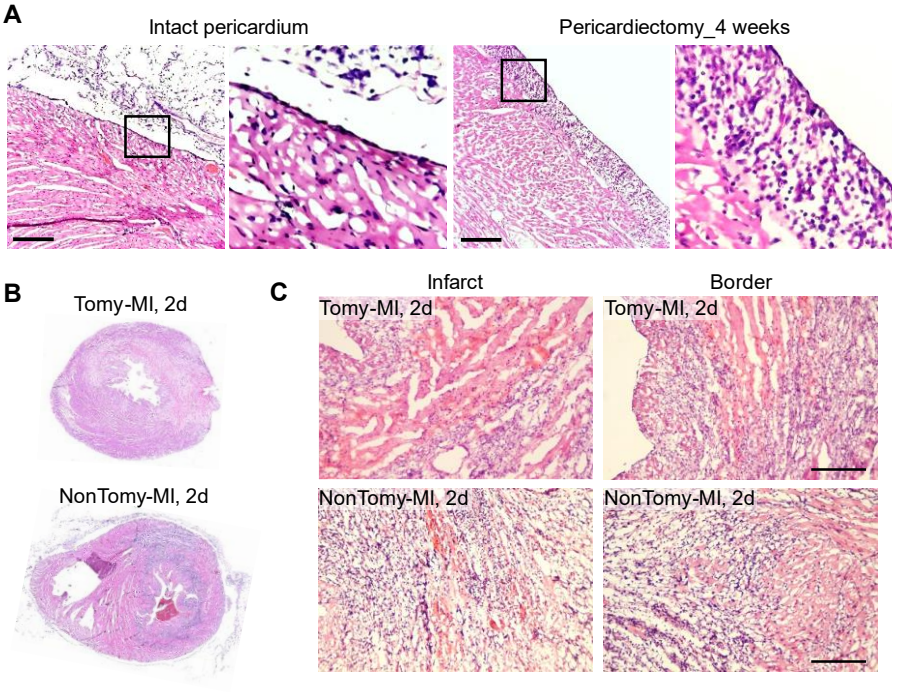

Fig. S4. Cardiac histological analysis following pericardium removal. (A) Pericardiectomy resulted in epicardial hyperplasia in normal rat hearts (without LAD ligation). Scale bar, 100 μm. (B) Pericardiectomy caused persistent cardiac edema in post-MI rat hearts. (C) Pericardiectomy resulted in necrotic stack in post-MI rat hearts. Scale bar, 100 μm.

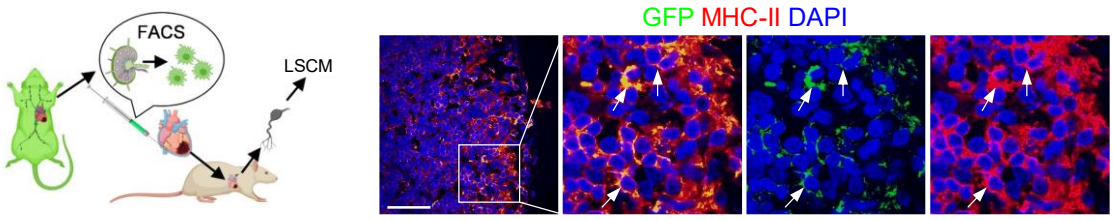

Fig. S5. Detection of GFP$^+$ antigen-presenting cells in the cardiac draining MLN. Immunofluorescence staining was performed to detect the distribution of GFP$^+$MHC-II$^+$ antigen-presenting cells in the mediastinal lymph node of wild type MI rats. The result indicated that pericardial drainage trajectory served as a direct path for antigen-presenting cells immigration towards the cardiac-draining mediastinal lymph node. Scale bar, 60 μm.

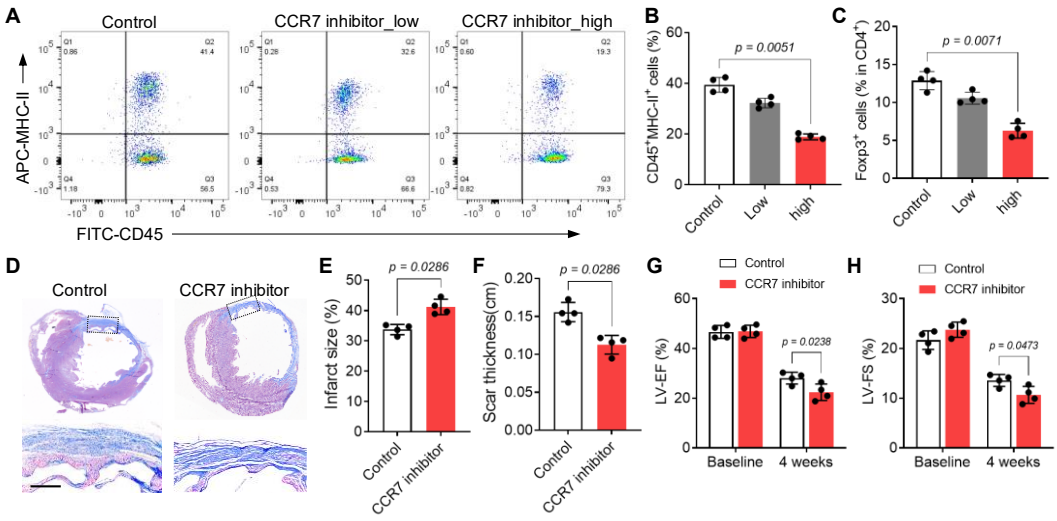

Fig. S6. Inhibition of APC migration worsened cardiac remodeling. (A, B) Flow cytometry detection of $CD45^{+}MHC\text{-}II^{+}$ APCs migration to MLN after iPC injection of 100 μL CCR7 inhibitor (cmp2105), with a low dose of 0.2mM and a high dose of 2mM. The control group received same volume of 5% DMSO. (B) The quantitative data of $CD45^{+}MHC\text{-}II^{+}$ APCs in MLN. n=4 animals for each group. (C) Detection of Treg ratios in MLN. n=4 animals for each group. (D-F) Cardiac histological analysis with Masson's trichrome stained sections. the infarct size(E) and scar thickness(F) were measured, respectively. Scale bar, 1mm. n=4 animals for each group. (G, H) Cardiac functional analysis. LV-EF and LV-FS were measured by echocardiography. n=4 animals for each group. All the quantitative data was shown as mean ± SD. *p* value was determined by Kruskal-Wallis's test with Dunn's correction for B, C; and by unpaired 2-tailed nonparametric Mann-Whitney test for E-H.

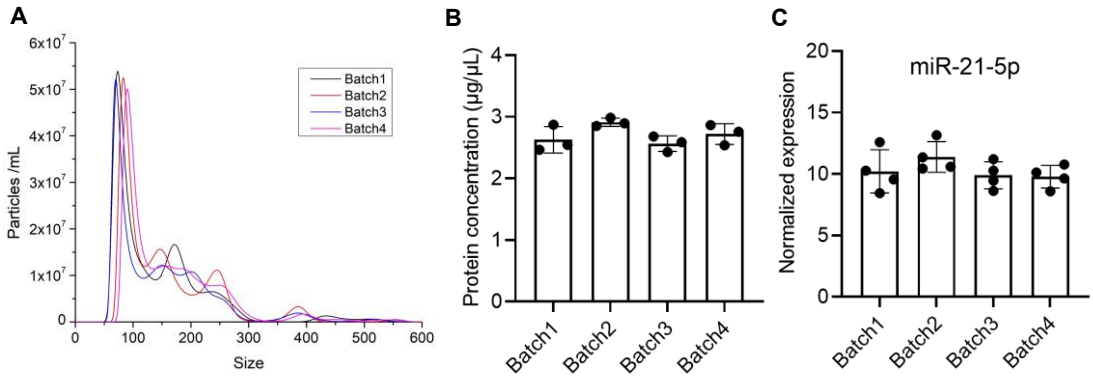

Fig. S7. Characterization of exosomes acquired from different batches. (A) Nanosight detection of exosomes size distribution. (B) Protein concentration detection. (C) Detection of miR-21-5p expression in the exosomes.

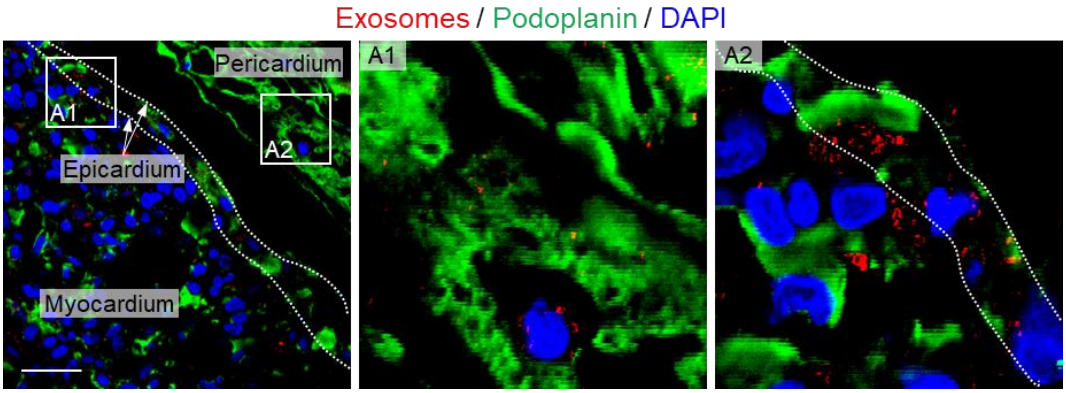

Fig. S8. Epicardial and pericardial uptake of exosomes after intrapericardial injection. DiD labelled exosomes were intrapericardially injected for myocardial infarction treatment. 2 days after injection, the uptake of exosomes by epicardial and pericardial cells were detected by immunofluorescence staining. Podoplanin was employed as a marker of epicardial and pericardial cells. Confocal imaging results indicated that intrapericardially injected exosomes can also absorbed by epicardial and pericardial cells. Scale bar, 60μm.

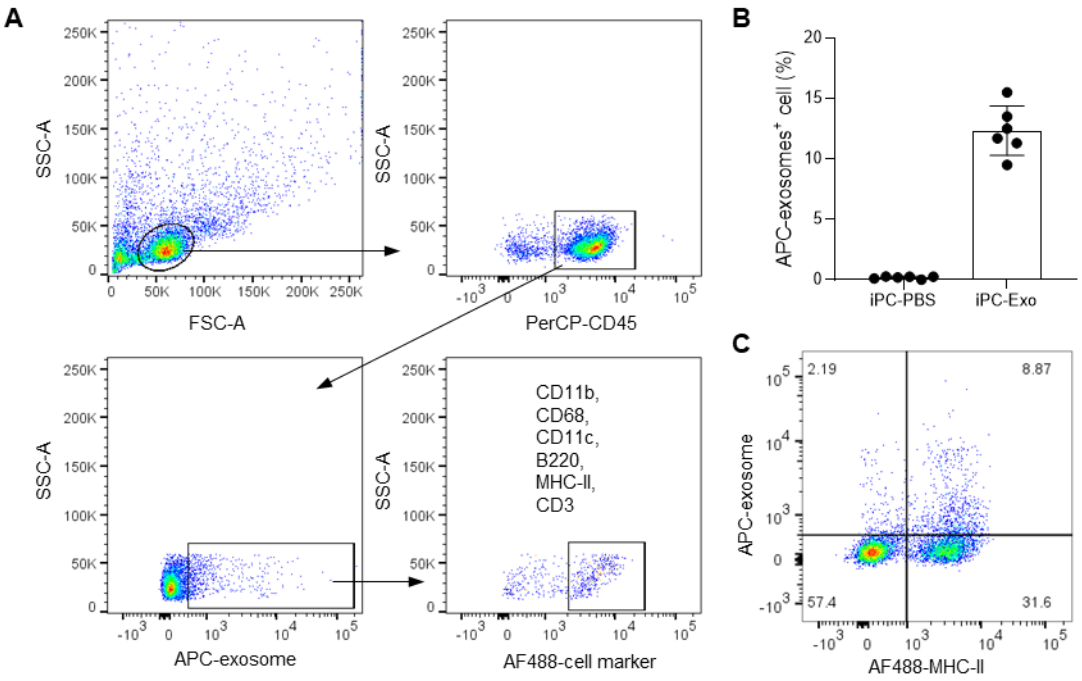

Fig. S9. Detection of exosomes uptake by cells in the mediastinal lymph node. (A) The gate strategy for analysis of exosomes uptake by specific cells in the mediastinal lymph node. **(B)** Quantification of exosomes^{+} cells in the mediastinal lymph node. Data was expressed as mean ± SD, n=6 animals for each group. **(C)** Detection of exosomes uptake by MHC-II^{+} antigen presenting cells.

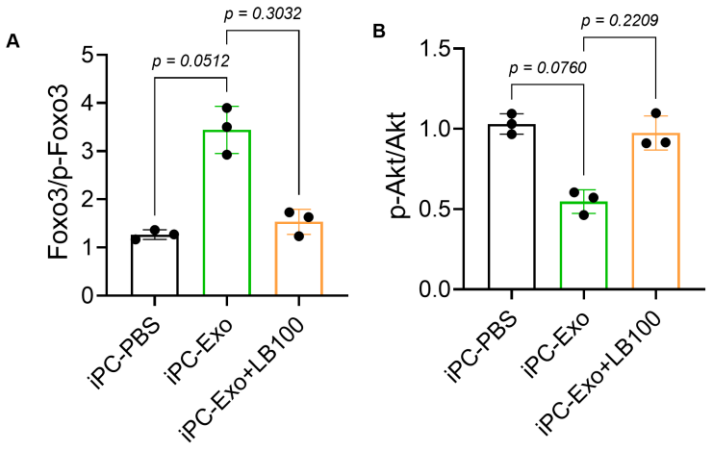

Fig. S10. Quantitative measurement of Foxo3/p-Foxo3 and p-Akt/total Akt ratios. The protein levels of Foxo3/p-Foxo3 and p-Akt/Total Akt were detected by western-blot, and accordingly, the indicated ratios were calculated by measuring optical intensity. Data was expressed as mean ± SD, n=triplicates for each group. *p* value was determined by Kruskal-Wallis's test with Dunn's correction.

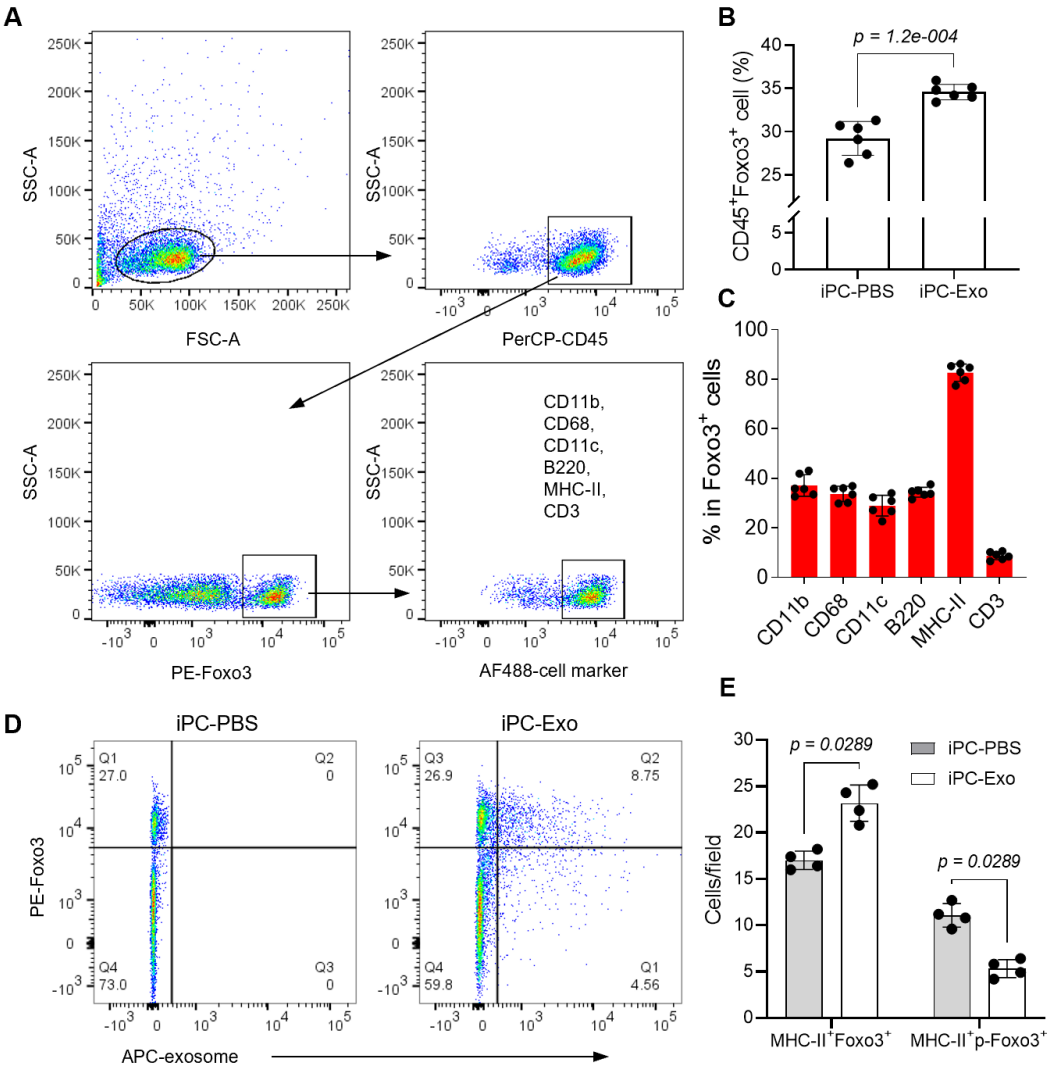

Fig. S11. Detection of Foxo3 expression in lymph node cells. (A) Gate strategy to detect the expression of Foxo3 by different cell types. **(B)** Quantitative data of $CD45^{+}Foxo3^{+}$ cells in the mediastinal lymph node. n=6 animals for each group. **(C)** Foxo3 expression in different type of cells. n=6 animals for each group. **(D)** Detection of foxo3 expression in cells that taking up exosomes. (**E**) Quantitative analysis of $Foxo3^{+}$ and p-$Foxo3^{+}$ antigen-presenting cells. n=4 animals for each group. All the quantitative data were expressed as mean ± SD. *p* value was determined by unpaired 2-tailed Student *t*-test for B, and nonparametric Mann-Whitney test for E.

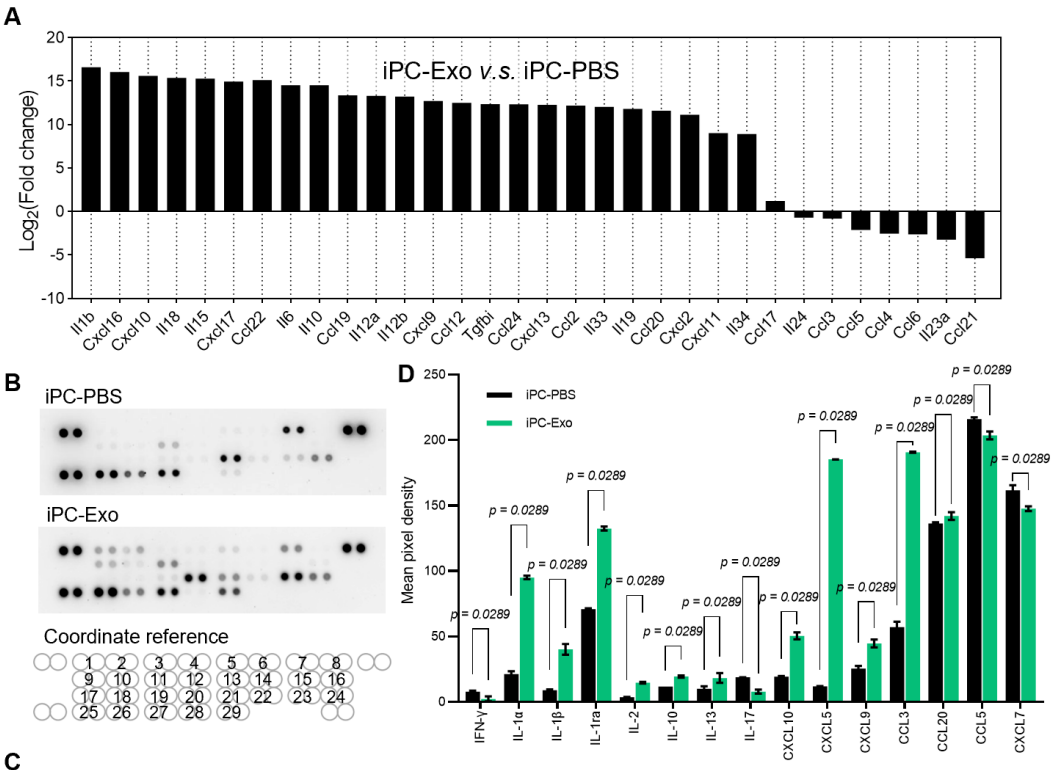

C

Ref. spot	CINC1	CINC2	CINC3	CNTF	CX3CL1	GM-CSF	CD54	IFN-γ	Ref. spot
	IL-1a	IL-1b	IL-1ra	IL-2	IL-3	IL-4	IL-6	IL-10	
	IL-13	IL-17	CXCL10	LIX	L-selectin	CXCL9	CCL3	CCL20	
Ref. spot	CCL5	CXCL7	TIMP1	TNF-a	VEGF			Negative control	

Fig. S12. Analysis of cytokine profiles. (A). RNA-seq analysis of cytokines expression in MHC-II^{+} antigen-presenting cells. (B) Cytokine array performed with whole lymph node lysate. (C) The coordinate reference of cytokine list of the array. (D) Quantitative analysis of cytokine array data. n=triplicates for each cytokine. Data was shown as mean ± SD. *p* value was determined by unpaired 2-tailed nonparametric Mann-Whitney test for D.

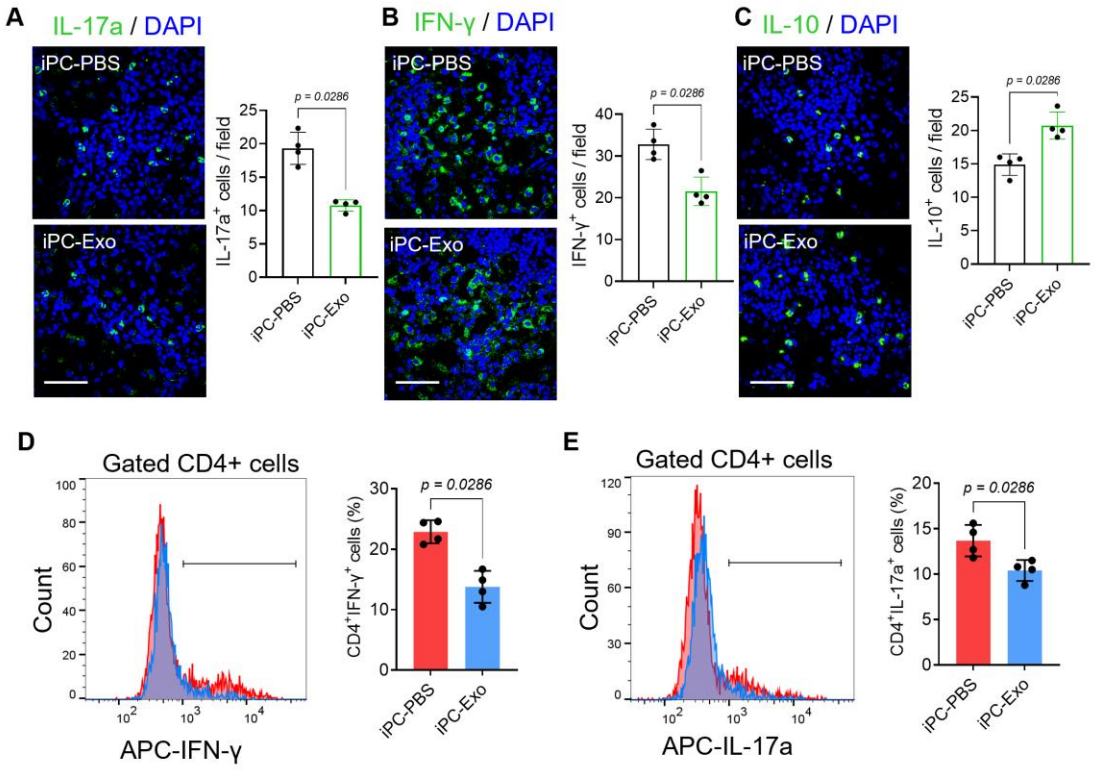

Fig S13. Analysis of T cell subtypes in the mediastinal lymph node. (A-C) Immunostaining of IL-17a, IFN-γ and IL-10 expression in the mediastinal lymph node and quantitative data. n=4 animals for each group. Scale bar, 60μm. (D-E) Flow cytometry detection of Th1 (IFN-γ^+) and Th17 (IL-$17a^+$) cell populations in the mediastinal lymph node and the quantitative data. n=4 animals for each group. All the quantitative data were shown as mean ± SD, *p* value was determined by unpaired 2-tailed nonparametric Mann-Whitney test for A-E.

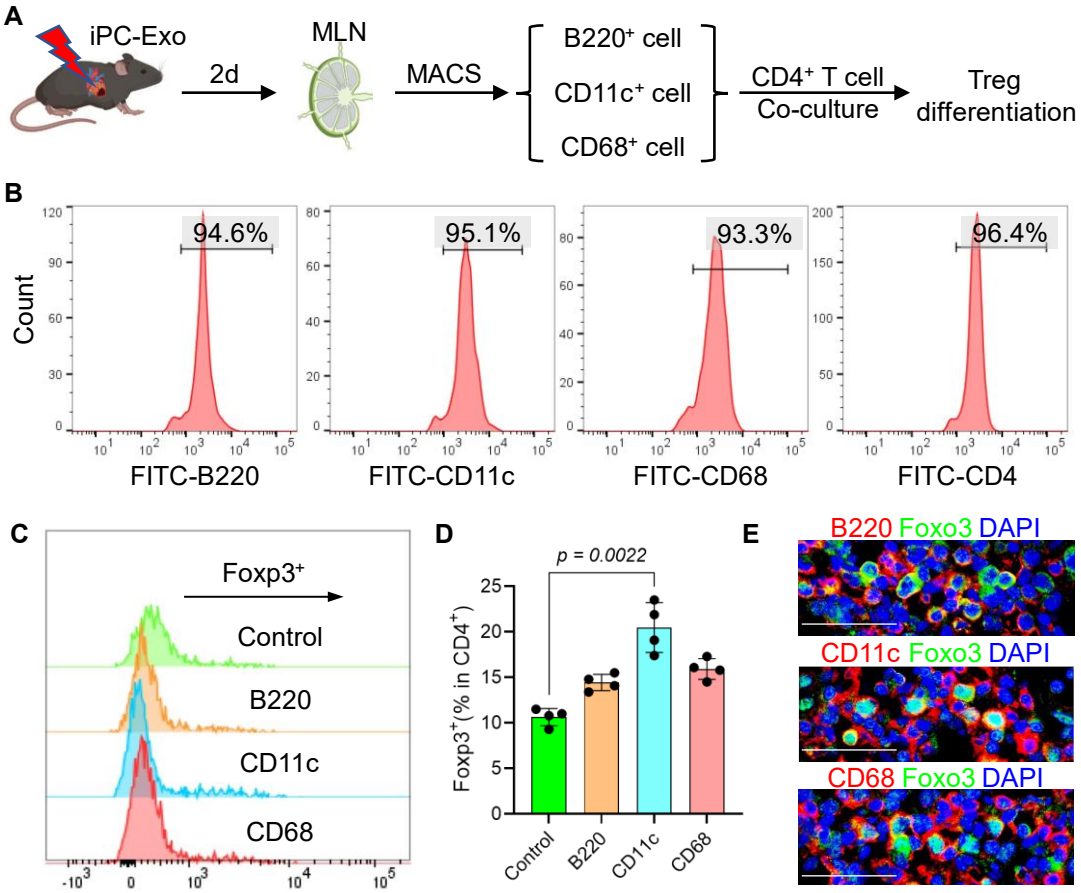

Fig. S14. *In vitro* study of Treg induction by APC cells. (A) Schematic study design. The single cell suspension was prepared from mediastinal lymph node (MLN) of MI rats received iPC-Exo treatment. Then the cells went through magnetic-activated cell sorting (MACS) to separate $B220^+$, $CD11c^+$, and $CD68^+$ subpopulations; these cells were then used for coculture with $CD4^+$ T cells, with a ratio of 2:1. $CD4^+$ T cells were sorted from non-injured rat MLN. The differentiation of Treg cells was then characterized by flow cytometry. (B) Flow cytometry detection of cell purity after MACS. (C) Histogram of $Foxp3^+$ Tregs in gated $CD4^+$ T cells. (D) Quantitative data of Treg cell ratios in $CD4^+$ T cells. n=4 independent tests for each group. Data were shown as mean ± SD, *p* value was determined by Kruskal-Wallis's test with Dunn's correction. (E) Immunofluorescence staining of Foxo3 in MLN confirmed the expression of Foxo3 by $B220^+$, $CD11c^+$ and $CD68^+$ cells. Scale bar, 40μm.

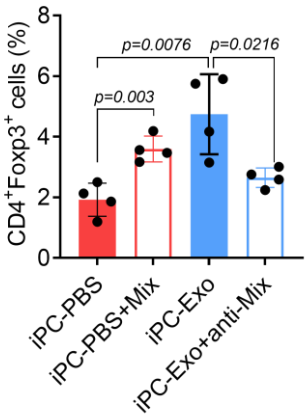

Fig. S15. Detection of cardiac infiltration of Tregs after cytokines (IL-10, IL-33 and IL-34) modulation. Cardiac infiltration of Tregs was measured by flow cytometry. Injection of cytokine mix (IL-10, IL-33 and IL-34) increased the cardiac deployment of Tregs, whereas injection of neutralizing antibody cocktail (anti-Mix) reduced cardiac infiltration of Tregs. Data were shown as mean ± SD, n=4 animals for each group. *p* value was determined by Kruskal-Wallis's test with Dunn's correction.

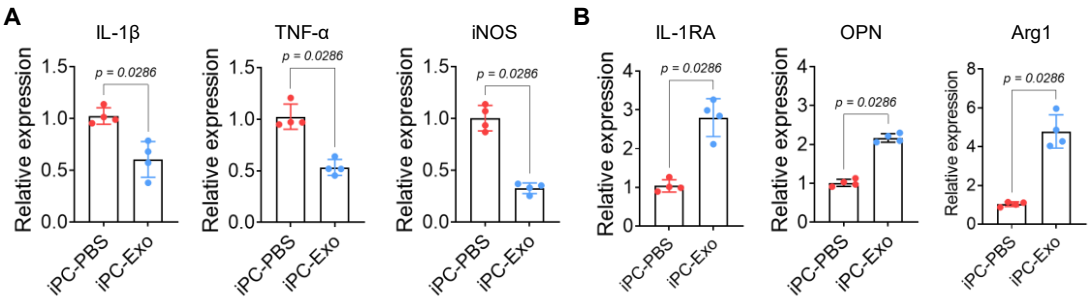

Fig. S16. qRT-PCR detection of macrophage related cytokines expression. (A) qRT-PCR detection of pro-inflammatory cytokines (IL-1β, TNF-α and iNOS) expression in the injured myocardium. (B) qRT-PCR detection of anti-inflammatory cytokines (IL-1RA, OPN and Arg1) expression in the injured myocardium. The value was normalized to the mean of the iPC-PBS group. Data were shown as mean ± SD, n=4 animals for each group. *p* value was determined by unpaired 2-tailed nonparametric Mann-Whitney test for A, B.

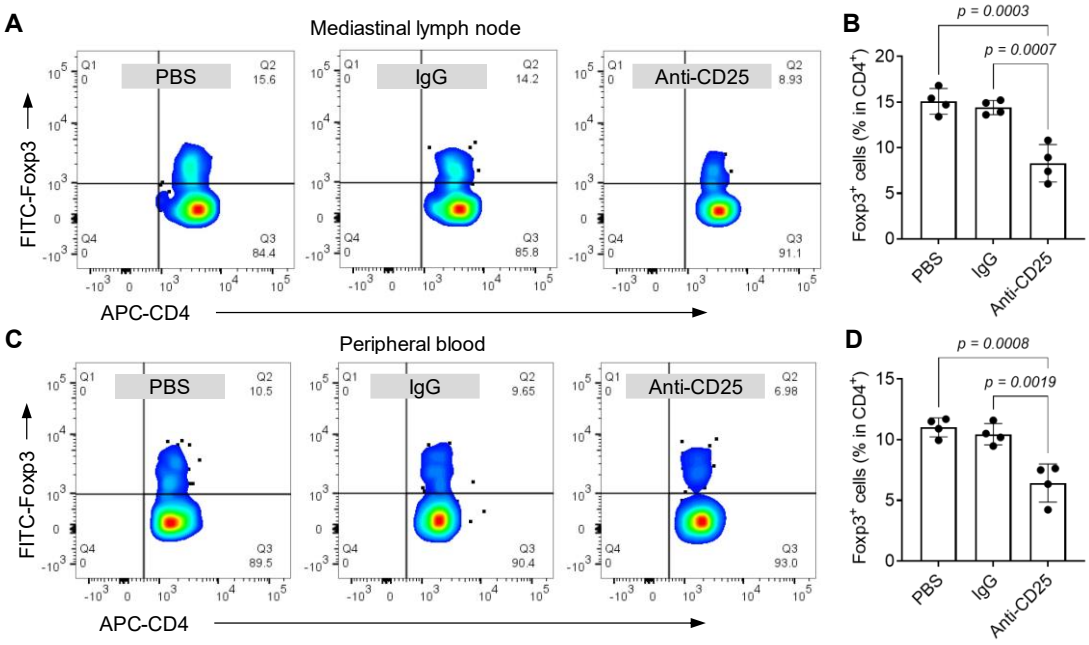

Fig. S17. Detection of Tregs in mediastinal lymph node and peripheral blood after depletion by using anti-CD25 antibody. (A) Detection of Tregs in mediastinal lymph node (MLN) after anti-CD25 antibody mediated Treg depletion, and (B) the quantitative data. n=4 animals for each group. (C) Detection of Tregs in peripheral blood after anti-CD25 antibody mediated Treg depletion, and (D) the quantitative data. n=4 animals for each group. Quantitative data was shown as mean ± SD. *p* value was determined by Kruskal-Wallis's test with Dunn's correction for B, D.

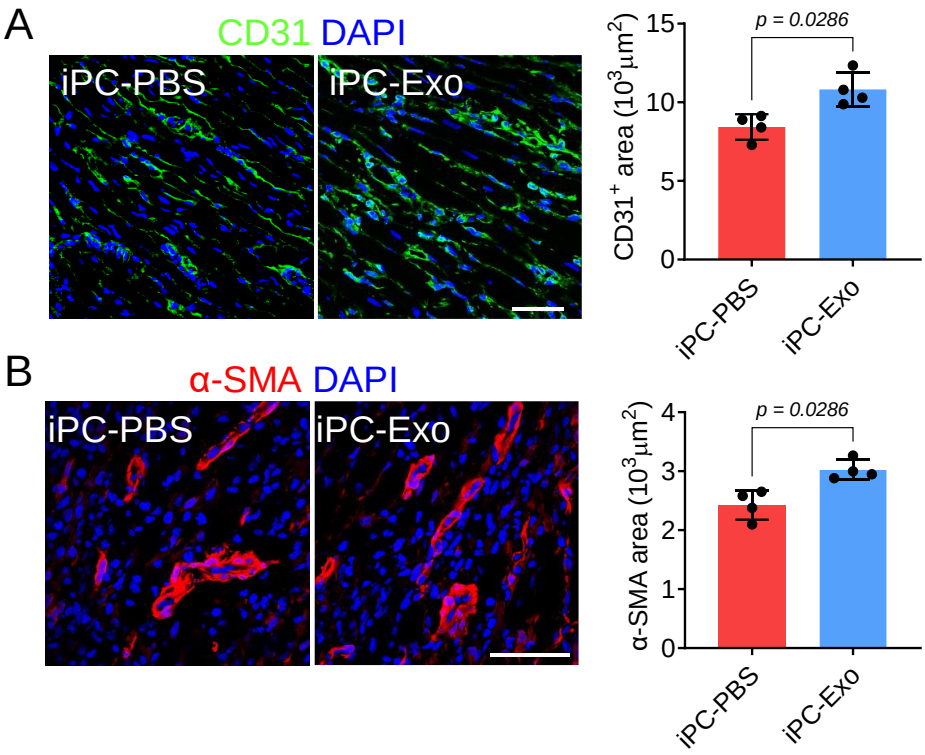

Fig. S18. MSC-exosomes treatment promoted vascular regeneration. (A) Detection of CD31 expression in the myocardium by immunostaining and the corresponding quantitative data. Scale bar, 60μm. (**B**) Detection of α-SMA expression in the myocardium by immunostaining and the corresponding quantitative data. Scale bar, 60μm. Data were shown as mean ± SD, n=4 animals for each group. *p* value was determined by unpaired 2-tailed nonparametric Mann-Whitney test for A, B.

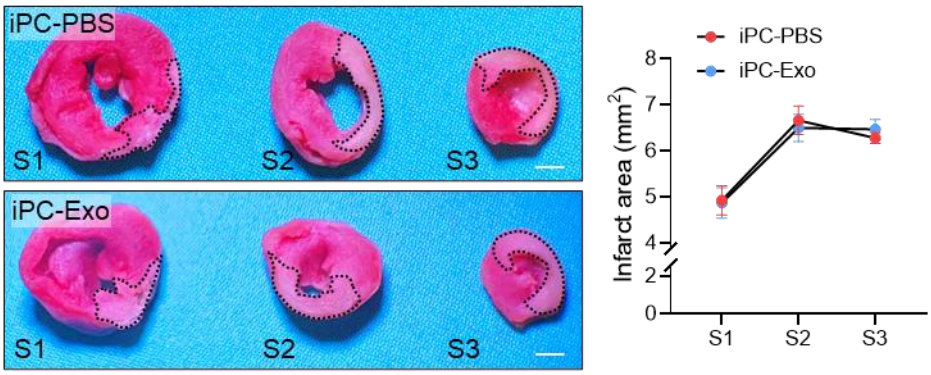

Fig. S19. TTC staining to show the initial infarct area. The initial infarct was measured 1 day after modeling. The quantitative data showed comparable initial infarct area between groups.

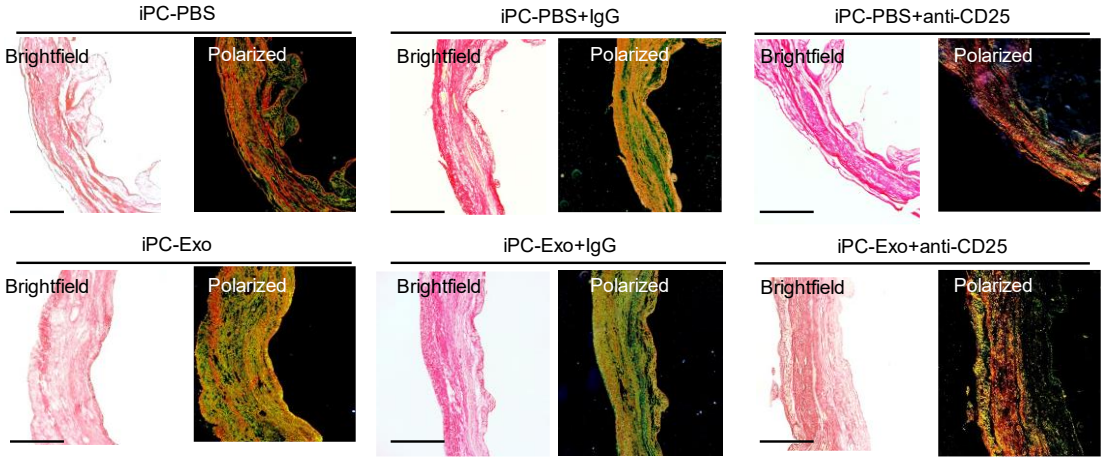

Fig. S20. MSC-exosomes treatment improved cardiac remodeling. Picrosirius red staining was performed to show the deposition of collage 1 and collagen 3 in the infarct scar. Scale bar, 1mm.

Supplemental Table 1. Primer sequence.

Primer	Sequence (Forward)	Sequence (Reverse)
Arg1	GTCTGTGGGAAAAGCCAATG	TTGCCATACTGTGGTCTCCA
IL-1RA	GGGAAAAGACCCTGCAAGA	GTGGATGCCCAAGAACACA
OPN	GACGGCCGAGGTGATAGCTT	CATGGCTGGTCTTCCCGTTGC
IL-1β	TGACCCATGTGAGCTGAAAG	AGGGATTTTGTCGTTGCTTG
TNF-α	GCCCACGTCGTAGCAAAC	GCAGCCTTGTCCCTTGAA
iNOS	GCTACGCCTTCAACACCAA	GCTTGTAACCACCAGCAGT
IL-35	ATGGCTAGGCTCTGTGCTTTC	TGGGCATCCACCTTCTCC
IL-33	CCCTGAGCACATACAACGACC	CACCATCAGCTTCTTCCCATC
IL-13	TCTGTGCAGCCCTGGAAT	GCGGAAAAGTTGCTTGGA
IL-10	GCAGGACTTTAAGGGTTACTTGG	GGGGAGAAATCGATGACAGC
GAPDH	TTCAACGGCACAGTCAAGG	CTCAGCACCAGCATCACC

Supplemental Table 2. Antibody information.

Antibodies	Catalog #	Species	Dilution
MPO	PA5-16672 (Thermo Fisher)	Rabbit	1:100
α-Sarcomeric actinin (α-SA)	ab9465 (Abcam)	Mouse	1:100
CD3	ab16669 (Abcam)	Rabbit	1:100
CD11c	PA5-90208 (Thermo Fisher)	Rabbit	1:100
CD11b	ab52478 (Abcam)	Rabbit	1:200
SOCS3	ab16030 (Abcam)	Rabbit	1:200
CD206	ab64693 (Abcam)	Rabbit	1:200
Ki67	11-5698-82 (Thermo Fisher)	Rat	1:100
MHC-II	ab55152 (Abcam)	Mouse	1:200
CD45	ab10558 (Abcam)	Rabbit	1:100
CD4	ab237722 (Abcam)	Rabbit	1:100
Foxp3	53-4776-42 (Thermo Fisher)	Rat	1:100
CD31	ab28364 (Abcam)	Rabbit	1:50
α-SMA	ab32575 (Abcam)	Rabbit	1:200
PP2A	ab32065 (Abcam)	Rabbit	1:1000(WB)
Foxo3-p253	ab47285 (Abcam)	Rabbit	1:100(IF); 1:500(WB)
Foxo3	ab70135 (Abcam)	Rabbit	1:100(IF); 1:500(WB)
p-Akt	4060S (Cell signaling technology)	Rabbit	1:1000(WB)
IL-17a	11-7177-81 (Invitrogen)	Mouse	1:100
IFN-gamma	559498 (BD Biosciences)	Mouse	1:100
IL-10	562156 (BD Biosciences)	Mouse	1:100
actin	MA5-11869 (ThermoFisher)	Mouse	1:1000(WB)
IL-34 Antibody	AF5159 (R&D)	Sheep	Neutralizing
IL-33 Antibody	PA5-47007(ThermoFisher)	Goat	Neutralizing
IL-10 Antibody	16-7102-85(ThermoFisher)	Rat	Neutralizing